The Preparation of Silica Supported, Dilute Limit PdAu Alloys via Simultaneous Strong Electrostatic Adsorption

Journal:	*Catalysis Science & Technology*
Manuscript ID	CY-ART-09-2022-001662.R1
Article Type:	Paper
Date Submitted by the Author:	30-Mar-2023
Complete List of Authors:	Dong, Anhua; University of South Carolina , Department of Chemical Engineering Shakouri, Abolfazl; University of South Carolina, Chemical Engineering Karakalos, Stavros; University of South Carolina, College of Engineering and Computing Blom, Douglas; University of South Carolina, Williams, Christopher; University of South Carolina, Chemical Engineering Regalbuto, John; University of South Carolina , Department of Chemical Engineering

The Preparation of Silica Supported, Dilute Limit PdAu Alloys via Simultaneous Strong Electrostatic Adsorption

Authors: *Anhua Dong, Abolfazl Shakouri, Starvros Karakalos, Doug Blom, Chris Williams, John R. Regalbuto**

Affiliations: Department of Chemical Engineering, University of South Carolina, Columbia, SC, 29208

ABSTRACT

Supported, dilute Pd-in-Au alloyed nanoparticles might possess enhanced reactivity due to the altered structural and electronic properties of the Pd atoms isolated in an Au nanoparticle matrix. Simultaneous strong electrostatic adsorption (co-SEA) is a promising approach to synthesize such nanoparticles at high metal dispersion. In this study, Pd sites diluted in Au nanoclusters were achieved via co-SEA with dilute Pd/Au concentration ratios of the impregnating

solution. X-ray diffraction, CO chemisorption, and scanning transmission electron microscopy (STEM) demonstrated ultrasmall nanoparticles (~1.7 nm) with homogenous alloying. Quantitative analysis of CO adsorption with Fourier-transform infrared spectroscopy was used to diagnose the disappearance of contiguous Pd surface ensembles with increasing dilution. Exclusively isolated Pd sites were achieved at or below the ratio of Pd/Au=0.04. Catalysts comprising completely isolated Pd exhibited turnover frequencies up to two orders of magnitude higher than pure Pd or Au catalysts.

Key words: heterogenous catalysts, strong electrostatic adsorption, dilute limit alloys, FTIR, isolated palladium sites, partial oxidation of 1-phenylethanol.

1 INTRODUCTION

Interest has arisen for heterogenous catalysts comprising single atom alloys (or dilute limit alloys, DLAs), in which one metal atom is diluted in the matrix of another supported metal nanoparticle, due to potentially enhanced catalytic activity, stability or other improved properties of the isolated atom [1-3]. For example, the isolation of noble metal atoms in a non-precious metal inert matrix enables the maximum noble metal utilization. Furthermore, DLA catalysts might combine the traditional advantages of alloys and single atom materials. Active metal coordination and the change in the electronic characteristics is intimately correlated to the interactions with the adsorbates, which in turn influence the catalytic performance. Numerous papers report tuned electronic properties of DLA catalysts by tailoring the atomic ratios, which are intimately related

to the reactivity. It has been reported that CO could bind more weakly on isolated Pt sites in Cu nanoclusters than on Pt ensembles/monometallic nanoparticles, which could improve CO-tolerance stability or thermal stability [4, 5]. Zhang et al. [6] affirmed the altered hydrogenolysis reaction pathway from dehydrogenation to dehydration over isolated Pt-Cu catalysts. Chen and Zhan[7] overviewed the electronic structure of DLA catalysts, and concluded that a combination of a lower density of state near the Fermi level, narrowing in the valence bands, and charge transfer have a tremendous effect on the adsorption behavior of reactants/intermediates in the catalytic processes. Similarly, Pei et al. [8] reported that excess electrons on the surface Pd monomers from the alloyed Ag matrix boosted the catalytic performance in acetylene hydrogenation. Density functional theory (DFT) simulation has also shown charge transfer in the dilute limit alloys, which influences the adsorption strength of various species [9].

Catalysts with isolated Pd sites anchored on the surface of Au nanoparticles have shown with initial promise for many reactions such as hydrogenation, dehydrogenation, oxidation, C-C coupling, etc. [10-13]. For example, Liu and colleagues [14] reported that a small amount of Pd in Au nanoparticles improved the activity of Au in the hydrogenation of 1-hexyne by nearly 10-fold, while at the same time retaining its high selectivity. It is proposed that the isolated Pd atoms on

the Au surface facilitated hydrogen dissociation and banded CO and H atoms more weakly. Indeed, Lee et al. [15] recently reviewed the available literature, and noted that dilute alloy catalysts with isolated atom or small ensembles in Cu, Ag, or Au host metals generally showed highly selective and enhanced hydrogenation activity. These effects are not limited to hydrogenation, as Wrasman et al [16] have shown that dilute Pd in Au alloy nanoparticles can generate the active oxidant in selective alcohol oxidation. This effect occurs even on even on inert carbon support due to the increased hydrogen dissociation ability of the isolated Pd sites in Au. Finally, it has been also reported that DLA catalysts with isolated metal sites showed enhanced anti-coking and/or CO poisoning resistance [4, 13].

A facile and generalizable method to synthesize supported single atom or dilute limit alloys with high metal dispersion and controlled composition will benefit efforts to explore these materials. Current preparation techniques most frequently include vacuum physical deposition (VPD), galvanic displacement, sequential reduction (SR), and co-precipitation or deposition-precipitation [14, 17]. Each of these methods has drawbacks; VPD is equipment-intensive, subject to impurities and not so scalable, while SR and precipitation methods involve incipient impregnation

89 or colloidal synthesis, which normally produce large particles. Galvanic displacement is possible
90 for only a limited number of metal systems.

91 We have previously demonstrated that simultaneous electrostatic adsorption (co-SEA) is
92 an effective method to synthesize highly-dispersed and well-alloyed bimetallic nanoparticles
93 (~1nm) with 1:1 atomic ratios [18]. This simple method can be applied to a wide variety of metal
94 precursors and oxide and carbon supports [19]. The synthesis of dilute limit alloys can be achieved
95 simply by controlling the concentrations of metal precursors in the impregnating solution. We
96 have recently employed the co-SEA synthesis of dilute Pd-in-Cu alloys on silica has been
97 successfully achieved, demonstrated by rigorous fitting and DFT interpretation of the Fourier-
98 transform infrared (FTIR) spectra of adsorbed carbon monoxide [20].

99 In this work, we extend co-SEA to the synthesis of a series of silica supported DLA
100 nanoparticles of Pd isolated in Au. With a comprehensive battery of characterization, we combine
101 *in-situ* IR spectroscopy and chemisorption to probe the isolation of surface Pd sites in Au
102 ensembles and the fraction of surface Pd. Powder X-ray diffraction (XRD) and scanning
103 transmission electron microscopy (STEM) measurements reveal particle size and the homogeneity
104 of PdAu alloying. *In-situ* X-ray photoelectron spectroscopy (XPS) reveals electronic interactions

between the two metals. The DLA series was finally characterized by evaluating the reactivity for the partial oxidation of 1-phenylethanol, showing significant improvement in activity.

2 EXPERIMENTAL

2.1 Materials

Aerosil 300 (A300) from Evonik Corporation was used as amorphous silica support with the surface area of 283 m^2/g. The point of zero charge (PZC) of A300 is 3.6 and water-accessible pore volume is 3.2 ml/g. Tetraamminepalladium (II) nitrate solution (99.99%, Sigma-Aldrich) ($PdTANO_3$) and gold ethylenediamine $Au(en)_2Cl_3$ (AuBen) was used as the cationic Pd and Au precursor, respectively. AuBen was made from tetrachloroauric (III) acid trihydrate (99.9%, Alfa Aesar) according to the reported literature [21, 22]. Other chemicals in AuBen preparation involve diethyl ether (99.9%, VWR), ethylenediamine (99%, Alfa Aesar) and anhydrous ethanol (>99.5, sigma-aldrich). NaOH and HCl were used to adjust the solution pH, which were supplied by VWR.

2.2 Adsorption Surveys and Catalysts Preparation

To explore the adsorption of Pd and Au precursors on silica during co-SEA, uptake surveys versus pH of cationic $[Pd(NH_3)_4]^{2+}$ and $[Au(en)_2]^{3+}$ complexes were performed with initial concentrations Pd and Au of 100 ppm and the silica surface loading (SL) at1000 m^2/L. The detailed

catalysts synthesis procedures were illustrated in our previous investigation [18-20]. Uptake results, plotted in Fig.1, show volcano-shaped uptake characteristic of electrostatic adsorption. Maximum Pd adsorption reached ~1.0 μmol/m^2 (3.7 wt%) at the optimal pH of 10-11, while a plateau from pH of 8.5 to 11.4 was observed in Au adsorption due to Au depletion; the surface density of this 0.62 μmol/m^2 corresponds to a loading of 4.1 wt% Au. The Au loading for the DLA series was targeted at 2.3 wt% Au.

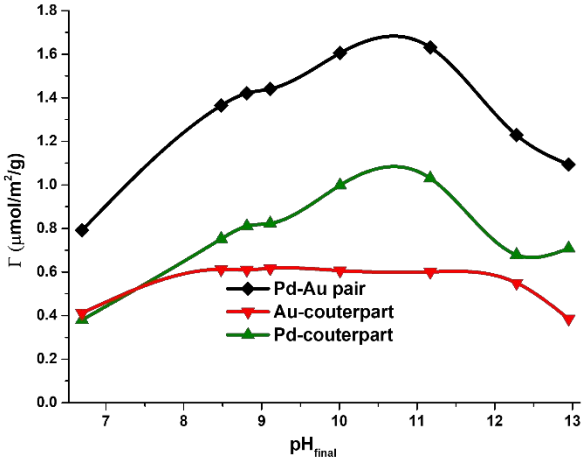

Figure 1. Uptake survey of Pd-Au pairs.

The synthesized series, including the electrostatic adsorption of hydrated Pd and Au cationic complexes onto the deprotonated and negatively charged silica surface is depicted in Scheme 1. It is presumed that drying and reduction in hydrogen leads to nanoparticles of the same composition as the adsorbed layer of well-mixed precursors.

133

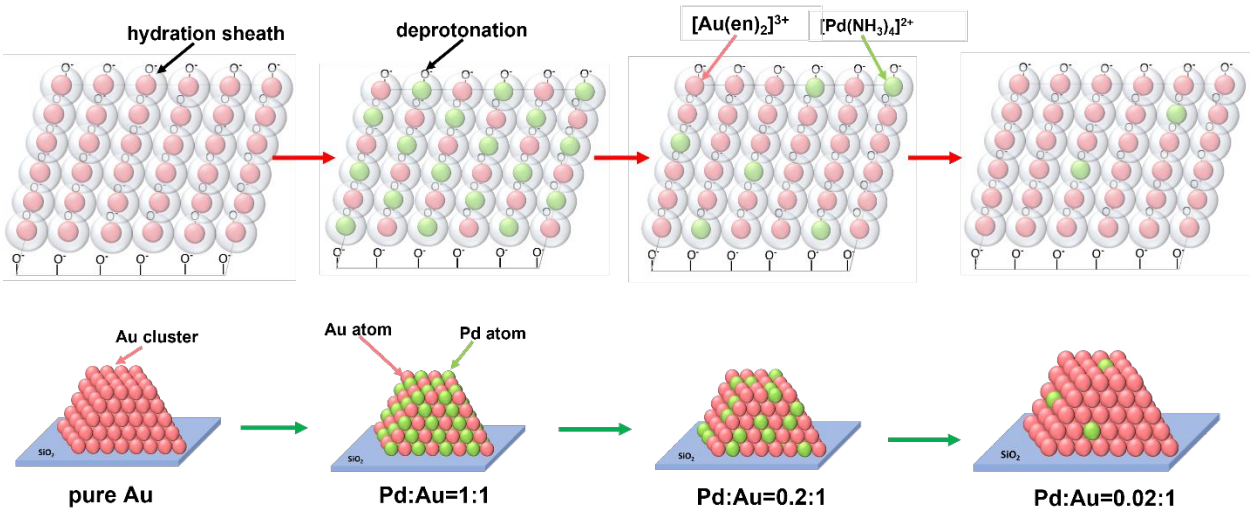

134

135 **Scheme 1.** Electrostatic adsorption of Pd, Au precursor complexes on silica support (a); palladium

136 and/or Pd-Au alloy formed on gold clusters after H_2 reduction (b).

137 Actual molar Pd/Au ratios of of 1.27:1, 0.23:1, 0.080:1, 0.040:1, 0.020:1, 0.012:1 and

138 0.010:1 were obtained by controlling Pd concentrations as listed in Table 1. The mass of Pd was

139 diluted from 1.54 wt% to 0.01 wt%. The initial pH of the 0.34 L metal precursor solution was

140 adjusted to around 11.5, then 1.2 g silica support was added resulting in a pH shift down to about

141 10.5 in all cases, in the optimal pH range for strong electrostatic adsorption as seen in Figure 1.

142 The slurry was placed on an orbital shaker for 1 hour and then vacuum filtered to obtain the powder

143 catalysts. Five ml aliquots of precursor solution were taken before and after contacting the support

144 to determine the loadings of Pd and Au as measured by ICP-OES (PerkinElmer Optima 2000 DV).

For the sake of comparison, monometallic Pd, Au catalysts were produced by SEA and one bimetallic catalyst (Pd/Au=0.02:1) was made by simultaneous dry impregnation (co-DI). For the latter preparation, appropriate amounts of metal precursors were dissolved into 3.84 ml DI water, which was the water accessible pore volume of 1.2 g of the silica support. As a control, pure silica support was treated in a metal free ethylenediamine aqueous solution to simulate the SEA procedure in the absence of metals.

The wet powders were dried at room temperature for 48 hours in darkness, and then reduced in a horizontal reduction furnace at 400 °C for 1 hour at the ramp rate of 5 °C in 250 sccm of 20% H_2 in N_2. The co-SEA prepared catalysts were denoted as Pd_xAu_1, where x is the molar ratio of Pd/Au. In the labels of the monometallic catalysts, the subscripts indicate the metal loadings. The sample labelled as $Pd_{0.02}Au_1$_co-DI were produced by dry impregnation.

Table 1. Catalysts information and concentrations of metal precursors in the synthesis.

Catalysts	**molar ratio**		**mass loading (wt%)**		**precursor conc. (ppm)**	
	Pd_x:Au_1	Pd_1:Au_y	Pd	Au	PdTA	AuBen
Pd_1Au_1	1:1	1:1	0.88	1.45	32	59
$Pd_{1.27}Au_1$	1.27:1	1:0.79	1.54	2.2	45	84

$Pd_{0.227}Au_1$	0.227:1	1:4.4	0.27	2.3	8.9	84
$Pd_{0.08}Au_1$	0.080:1	1:13	0.10	2.3	3.0	84
$Pd_{0.04}Au_1$	0.040:1	1:25	0.05	2.2	1.5	84
$Pd_{0.02}Au_1$	0.020:1	1:50	0.024	2.3	0.74	84
$Pd_{0.012}Au_1$	0.012:1	1:83	0.014	2.2	0.54	84
$Pd_{0.01}Au_1$	0.010:1	1:100	0.010	2.3	0.37	84
$Au_{2.2}$	0:1	0:1	---	2.2	0	84
Au_1	0:1	0:1	---	0.84	0	40
$Pd_{0.97}$	1:0	1:0	0.97	---	36	---
$Pd_{0.10}$	1:0	1:0	0.10	---	3.6	---
$Pd_{0.02}Au_1$_co-DI	0.020:1	1:50	0.024	2.3	92	8670

2.3 Catalyst Characterization

Temperature programmed reduction (TPR) was conducted in a Micromeritics 2920 equipped with a thermal conductivity detector. Fresh samples of around 200 mg were pretreated in Ar at 180 °C for 1 hour, cooled down to room temperature, switched to 10% H_2/Ar at flowrate of 50 sccm, and then increased to 800 °C at a ramp of 5 °C/min.

Powder X-ray diffraction (XRD) was carried out with a Rigaku MiniFlex II with a high sensitivity D/teX Ultra Si slit detector. XRD patterns were recorded from 10-90° 2θ with 0.02°

step size using a Cu-Kα radiation source (λ =1.5406 Å) at 30 mA and 15kV. Fityk version 1.1.3 software was employed for silica background subtraction and Gaussian peak fitting. Average particle sizes were determined with the Scherrer equation with a shape factor of 0.94 [23].

Pulse CO-chemisorption was measured over PdAu DLA catalysts on a Micromeritics 2920 equipped with a TCD to quantify Pd sites on Au nanoparticles surface. All the measured samples were in-situ reduced in a U-tube installed into the equipment at 400 °C for 1 hour in 10% H_2/Ar at a ramp of 5 °C/min, cooled down to room temperature and then pulsed with 10% CO/He until the discretely injected gas volumes was unchanged by TCD. The difference between the amounts of injected CO and the measured residual amount in the gas effluent was used to calculate the amount of adsorbed CO on PdAu alloys. A small volume of CO was detected over the monometallic Au sample (0.05 cm^3/g_{cat}), which was then subtracted from the DLA catalysts to determine the population of adsorbed CO on Pd. The stoichiometry of CO/Pd derived from CO-FTIR analysis was applied to estimate Pd dispersion.

An aberration corrected JEOL 2100F scanning transmission electron microscopy (STEM) was employed to obtain average particle sizes and size distributions as well as to image the bimetallic nanoparticles at high magnification. Sample preparation involved ultra-sonicating the

catalyst powder in ethanol and adding a drop to the copper TEM grid supporting a holey carbon film. Particle size distributions were achieved with analysis class size of 1 Å based on at least 700 particles by using Particle 2 software. Number average particle sizes were calculated as $D_n=\sum n_iD_i/\sum n_i$ and the volume average size, for comparison with XRD, as $D_v ==\sum n_iD_i^4/\sum n_iD_i^3$ [24].

To probe the electronic structure and surface composition of the reduced PdAu DLA samples, X-ray photoelectron spectroscopy (XPS) was performed on a Kratos AXIS Ultra DLD XPS system with a monochromatic Al K source and a catalysis cell for in-situ pretreatment. Before procuring spectra, samples were in-situ reduced in the chamber at 180 °C for 1h in 20 %H_2. Binding energy was calibrated with the C1s peak at 284.8 eV [25] (and was consistent with using the Si 2p peak at 104.0 eV). With a subtraction of Shirley background, XPS spectra were fitted with XPS Peak 4.1 software by using a mixed Gaussian/Lorentzian function and fixing spin-orbit splitting area ratio.

Fourier-transform infrared spectroscopy (FTIR) with CO as probe molecule was employed to probe the atomic geometry of surface Pd sites. FTIR measurements were performed on a Thermo Electron model 4700 spectrometer in transmission mode with a liquid-nitrogen-cooled MCT detector. A cylindrical stainless-steel cell was used in all FTIR experiments for in-situ

197 pretreatment. After fine grinding, 15 mg sample was pressed into pellets in a diameter of 0.5 inch
198 under the pressure of 3 bar for 20s. The spectra were recorded in a single beam mode with a total
199 of 64 scans and a resolution of 4 cm^{-1} in the 4000-450 cm^{-1} spectral region. Prior to collect the
200 spectra, each sample was first reduced in 20% H_2/N_2 at 180 °C for 1 hour at the ramp of 5 °C/min,
201 cooled down to room temperature in N_2, with one spectrum collected and set as the background.
202 The lower reduction temperature was employed for the in-situ IR characterization as it completely
203 eliminated the adsorption of CO onto Au. Afterward, 1% CO/Ar was turned on and spectra were
204 collected until the sample was saturated with CO. Subsequently, 1% CO/Ar was switched by pure
205 N_2 to flush away the gas-phase and any physiosorbed CO. Meanwhile, spectra were acquired until
206 the signal of adsorbed CO signal stabilized.

207 Gaussian functions were used to resolve IR spectra subtracted that of the pure Au sample
208 by using Fityk software. Curve fitting was firstly conducted on monometallic Pd catalysts to
209 optimize the full width at half maximum (FWHM) in the Gaussian function and deconvoluted CO
210 bands position. In the deconvolution of IR spectra over PdAu DLA catalysts, the peak parameters
211 of monometallic Pd samples, including FWHM, height and position, were initially employed and
212 then optimization by principally by the peak height, and in some cases with small variations of the

213 peak position and FWHM. The deconvoluted peak area corresponded to varied CO bands were
214 used to calculate the fraction of linearly adsorbed CO molecules.

215 *2.4 Partial Oxidation of 1-Phenylethanol*

216 Catalysts were evaluated for the partial oxidation (or dehydrogenation) of 1-phenylethanol
217 (PE) to acetophenone in a 110 ml semi-batch reactor (Autoclave Engineers) at 50 psig of O_2 and
218 160°C, with a stirring rate of 400 rpm. In most cases, the initial reactor loading was 50 ml 1-
219 phenylethanol and 106 mg catalyst. Oxygen was provided to the reaction medium from the hollow
220 shaft of the impeller outlet holes above and below the liquid level (Dispersamax™, Autoclave
221 Engineers). Much attention was placed on ensuring the safety of the reaction. The reactor is
222 equipped with a rupture disk, as is standard for performing high pressure reactions. In addition, a
223 needle valve was installed to control O_2 flow to the reactor. This valve is opened only to the level
224 required to maintain the reaction pressure in the vessel. Thus, in the event of a thermal runaway,
225 the reactor will quickly become starved of oxygen, and the rate will be limited, providing the
226 opportunity to shut the system down. No evidence of any uncontrolled reaction was observed. The
227 compositions of liquid reactant and products at various reaction times were measured using a gas
228 chromatograph (HP 5890) with an HP-5 capillary column and a flame ionization detector coupled

to an autosampler. Turn over frequencies (TOFs) based on Pd or total metal (Pd+Au) were calculated according to the following equations:

$$\text{Conversion (\%)} = \frac{converted\ n_{PE}\ (mol)}{initial\ n_{PE}\ (mol)} * 100 \qquad \text{equation (1)}$$

$$\text{TOF}_{metal} = \frac{converted\ n_{PE}\ (mol)}{n_{metal}(mol) * reaction\ time\ (h)} \qquad \text{equation (2)}$$

3. RESULTS AND DISCUSSION

3.1 Catalyst Characterization

Temperature programmed reduction profiles for pure Au, Pd, and Pd/Au bimetallic nanoparticles (Figure S1) showed reduction of pure Au at about 145 °C and pure Pd via SEA at about 170 °C. A DI-derived Pd sample at the same loading gave a lower reduction peak, presumably due to weaker interaction of the precursor with the silica surface. The reduction temperature of the 1:1 Pd:Au sample lowered toward that of Au, and low ratios of Pd:Au looked similar to pure Au. The Au-containing samples contained positive peaks from 200 °C - 250 °C presumed to arise from the decomposition of the ethylenediamine ligand from the gold precursor [26]. This peak shifted downward in temperature with the addition of even small amounts of Pd and

in proportion to the amount of Pd added, which is an indication that the two metals are in intimate contact.

Powder XRD characterization of the PdAu DLA catalysts is shown in Figure 2. Raw diffractograms (Figure 2a) are for the support-only (bottom), 0.97 wt% Pd-only (second from bottom), the DLA series, and then Au-only pattern (top). Peaks from metal nanoparticles are very broad as the particle size is ultra-small; the (200) fcc peaks are seen as right-hand shoulders on the (111) peaks near 40° 2θ. With the high intensity detector employed, careful background subtraction and peak fitting allows the identification of nanocrystalline features even smaller than 1 nm [27]. The Pd-only sample exhibits discernable broad peaks (Figure 2b, bottom) which can be fit as 1 nm Pd_2O particles. The Au-only sample (top pattern of Figure 2a) can be fit with metallic fcc Au peaks with size 1.7 nm, however, the position of the (111) peak, at 39.1° 2θ, is about 0.83° 2θ higher than that expected for bulk Au. This can be explained by the lattice contraction of ultrasmall Au nanoparticles as has been firmly established by x-ray absorbance [28]. The rest of the samples, containing high to low amounts of Pd (bottom to top in Figures 2a and 2b) can all be fit with a single set of fcc (111) and (200) peaks.

The peak positions from the raw data, and peaks shifts with a correction for the lattice contraction of Au are shown in Figure 2c. The samples at higher Pd:Au ratios show an upward shift in 2θ which approaches pure Au at the lowest Pd ratios, and which deviates from the lattice contraction correction which should be constant given the constant Au matrix nanoparticle size. While no discernable alloying is evidenced at the lowest Pd ratios, above 0.04:1 Pd:Au an upward shift in peak position is consistent with adding a Vegard's law [29,30] correction to the lattice contraction which implies alloying of the metals, until the final ratio of 1:27:1, at which point the Au lattice contraction correction is not needed, possibly due to the presence of large amounts of Pd.

Particle sizes derived from the peak broadening are given in Table 2. All of the gold-rich catalysts have the same size (~1.7 nm) as the pure Au sample. The highest ratio of $Pd_{1.27}Au_1$ exhibited the smallest bimetallic particles of 1.4 nm. Pei et al[11] detected smaller bimetallic particles with even trace amounts of Pd in Au (from 4.2 nm to 2.8 nm) and concluded Pd promoted the thermal stability of Au nanoclusters which caused a stronger PdAu-silica interaction. Qian et al [31] also noticed smaller size of PdAu alloys with increased amount of Pd in fixed Au contents (from 4.0 nm to 2.3 nm) and ascribed it to the enhancement of Au dispersion by the alloy

formation. In contrast, sharp metallic [111] and [200] peaks appeared for a $Pd_{0.02}Au_1$_co-DI sample (Fig. S2), indicative of larger alloy particles. Peaking fitting reveals two sets slightly offset fcc peaks, indicating two alloy phases with the average particle size of 11 nm.

Pulse CO chemisorption was employed to address the question of how much Pd was on the surface, versus the amount in the bulk. Results are shown in Table 3 and are reported as uptake per gram of catalyst and per gram of Pd. If all Pd were on the surface the uptake would be 9.4 $\mu mol/g_{Pd}$. The Pd "dispersion" which in this case is the amount of Pd on the surface versus the amount of Pd in the bulk of the alloy phase, is seen to vary from about 54% to about 33%. From a Van Hardeveld and Hartog analysis[32] based on the XRD-determined particle size, the ratios of total metal dispersion, or the number of Au + Pd surface atoms versus total atoms is listed in the rightmost column of the table. That Pd dispersion is similar to the total metal dispersion suggests that co-SEA leads to the formation of bulk alloying with little or no surface enrichment. Surface enrichment of Pd is not expected, at least in the absence of a reactant which can pull it to the surface, as the surface free energy of Pd (2.403 J/m^2) is somewhat higher than that of Au (1.626 J/m^2) [33]. That the majority of the Pd goes into bulk alloying is consistent with the XRD data. Below

0.04:1 Pd:Au, while chemisorption indicates the absence of Pd from the nanoparticle surfaces, the amount of the Pd is too small to produce a measurable XRD peak shift.

297 Table 2. Particle size and bulk phase identified by XRD and STEM.

Samples	D_{XRD} (nm)	STEM		Bulk phase identified by XRD or STEM
		D_V (nm)	D_n (nm)	
$Pd_{0.97}$	0.98	1.2	0.97	Pd_2O (Pd in STEM)
$Pd_{1.27}Au_1$	1.4	1.3*	1.1*	Bulk alloy, speckled
$Pd_{0.227}Au_1$	1.7	---		Bulk alloy
$Pd_{0.08}Au_1$	1.7	---		Bulk alloy
$Pd_{0.04}Au_1$	1.7	2.1	1.5	Bulk alloy
$Pd_{0.02}Au_1$	1.7	---		Au
$Pd_{0.012}Au_1$	1.7	---		Au
$Pd_{0.01}Au_1$	1.8	---		Au
$Au_{2.2}$	1.7	2.0*	1.3*	Au

298 * STEM estimates for a Pd_1Au_1 sample.

299
300

301 Table 3. Pulse CO chemisorption over PdAu DLA catalysts.

Samples	Q_{CO}	Q_{Pd}	Pd dispersion	N_S/N_T*
	$cm^3/g_{cat.}$	$\mu mol/g_{Pd}$	%	%
$Pd_{1.27}Au_1$	0.809	5.1	54	48

$Pd_{0.227}Au_1$	0.211	4.3	46	38
$Pd_{0.08}Au_1$	0.067	3.3	36	38
$Pd_{0.04}Au_1$	0.043	3.9	41	39
$Pd_{0.02}Au_1$	0.017	3.1	33	39

302 * per Van Hardeveld and Hartog[32]

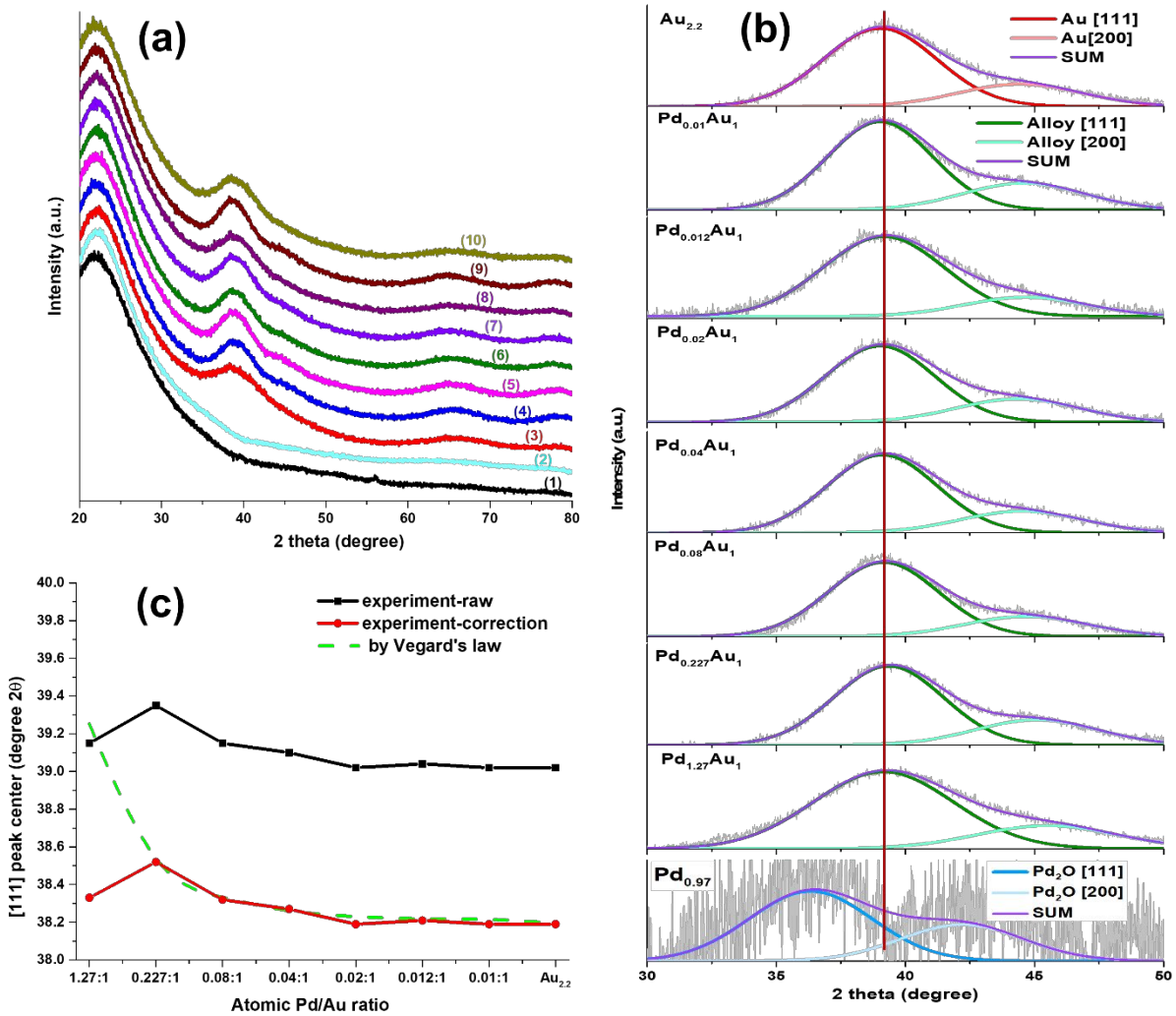

303

304 Figure 2. XRD analysis of the PdAu DLA series, a) Normalized XRD profiles for (1) treated SiO_2,

305 (2) $Pd_{0.98}$, (3) $Pd_{1.27}Au_1$, (4) $Pd_{0.227}Au_1$, (5) $Pd_{0.08}Au_1$, (6) $Pd_{0.04}Au_1$, (7) $Pd_{0.02}Au_1$, (8) $Pd_{0.012}Au_1$,

306 (9) $Pd_{0.01}Au_1$, (10) $Au_{2.2}$ catalysts, b) background-subtracted and fitted XRD patterns; c)
307 comparison of results with Vegard's law.

308

309

310

311 To gain further insight into the particle size and morphology, electron microscopy analysis
312 was performed on mono/bimetallic PdAu catalysts. Representative STEM images (Fig.3) revealed
313 regular spherical particles with tight size distributions. Particle size estimates from STEM (volume
314 averages) were largely consistent with XRD estimates as given in Table 3. Under the electron
315 beam, the pure Pd oxides would be reduced, so the size reported is assumed to be reduced and not
316 oxidized metal.

317 Careful inspection of high magnification images of the Pd_1Au_1 sample (Figure 3c) reveal
318 specked nanoparticles indicative of well-mixed alloys[34]. This effect is not seen (and is not expected
319 to be seen) at low Pd:Au ratio. To further investigate the isolation of a minority metal, PdAu
320 nanoparticles with inversed atomic Pd/Au ratio (1:0.04) were produced via the same synthetic
321 procedure of co-SEA on oxidized carbon and the microscopy images are presented in Fig. S3. The

clear occurrence of isolated, brighter Au atoms speckled throughout the dimmer Pd nanoparticles (in yellow circles) supports the hypothesis that electrostatic adsorption is an efficient methodology to attain DLAs through atomically distributing one minority element into another host metal atoms.

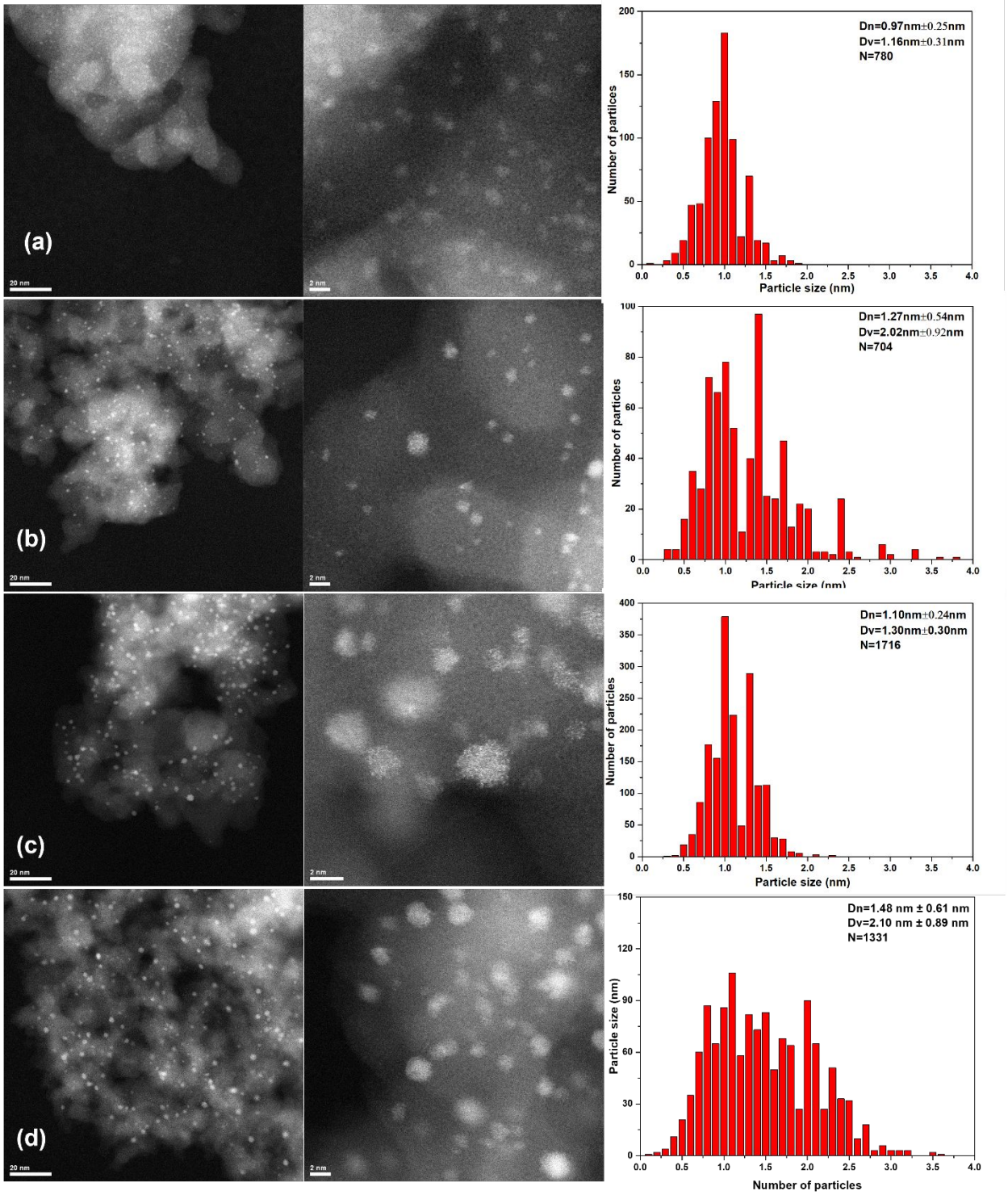
(a)
20 nm
2 nm
Dn=0.97nm±0.25nm
Dv=1.16nm±0.31nm
N=780
Number of partilces
Particle size (nm)
(b)
20 nm
2 nm
Dn=1.27nm±0.54nm
Dv=2.02nm±0.92nm
N=704
Number of particles
Particle size (nm)
(c)
20 nm
2 nm
Dn=1.10nm±0.24nm
Dv=1.30nm±0.30nm
N=1716
Number of particles
Particle size (nm)
(d)
20 nm
2 nm
Dn=1.48 nm ± 0.61 nm
Dv=2.10 nm ± 0.89 nm
N=1331
Particle size (nm)
Number of particles

325

Figure 3. STEM images of monometallic $Pd_{0.97}$_SEA (a), Au_1_SEA (b), Pd_1Au_1_co-SEA (c), and $Pd_{0.04}Au_1$_co-SEA (d) catalyst at low and high magnification as well as the particle size distribution histograms.

X-ray photoelectron spectroscopy (XPS) analysis was conducted after *in-situ* reduction to understand the electronic properties and surface composition. XPS Au4f, Pd3d, and Au4d core level spectra were deconvoluted by using two contributions originating from Pd^0 and Au^0, and are shown in Fig.4. Assignments of resolved XPS spectra and the derived chemical composition are listed in Table 4. $Au4f_{7/2}$ and $Au4d_{5/2}$ peaks were detected on monometallic gold sample at binding energy (B.E.) of 84.3 eV and 334.7 eV, respectively, in close agreement to reported values [35]. The obtained binding energy of Pd^0 counterpart over $Pd_{0.97}$ was located at 335.4 eV and 340.1 eV for $Pd3d_{5/2}$ and $Pd3d_{3/2}$, respectively, and the observed higher binding energy can be attributed to the small particles [36]. In PdAu DLA catalysts, with Pd dispersed in Au nanoparticles, Pd3d and Au4f binding energies moved in the opposite directions, with $Au4f_{7/2}$ going down from 84.3 eV for pure Au to 83.4 eV in the Pd_1Au_1 alloy and $Pd3d_{5/2}$ going up from 335.3 eV for pure Pd to 335.6 eV as it was diluted. These shifts evidence charge transfer from Pd to Au in the alloys due to a higher electronegativity of Au, and are consistent with the observations of many groups[14,33,35,37-39]. That

such small amounts of Pd exhibit an effect in the Au matrix can be explained by the very small size (1.7 nm by XRD) of the Au matrices, and assuming that the Pd is homogeneously distributed in the Au. Liu and colleagues [14] also detected charge transfer between Pd and Au on their carbon-supported PdAu alloys with trace amount of Pd (0.4 at.%).

Table 4.Binding energies of $Au4f_{7/2}$, $Pd3d_{5/2}$, and $Au4d_{5/2}$.

Samples	**Binding Energy (eV)**		
	$Au4f_{7/2}$	$Pd3d_{5/2}$	$Au4d_{5/2}$
$Pd_{0.98}$	---	335.3	---
Pd_1Au_1_co-SEA	83.8	335.5	334.2
$Pd_{0.227}Au_1$_co-SEA	83.8	335.6	334.2

$Pd_{0.08}Au_1$_co-SEA	83.8	335.6	334.2
$Pd_{0.04}Au_1$_co-SEA	83.8		334.2
$Pd_{0.02}Au_1$_co-SEA	84.0	weak Pd signal	334.4
$Pd_{0.01}Au_1$_co-SEA	84.3		334.6
Au_1	84.3	---	334.7

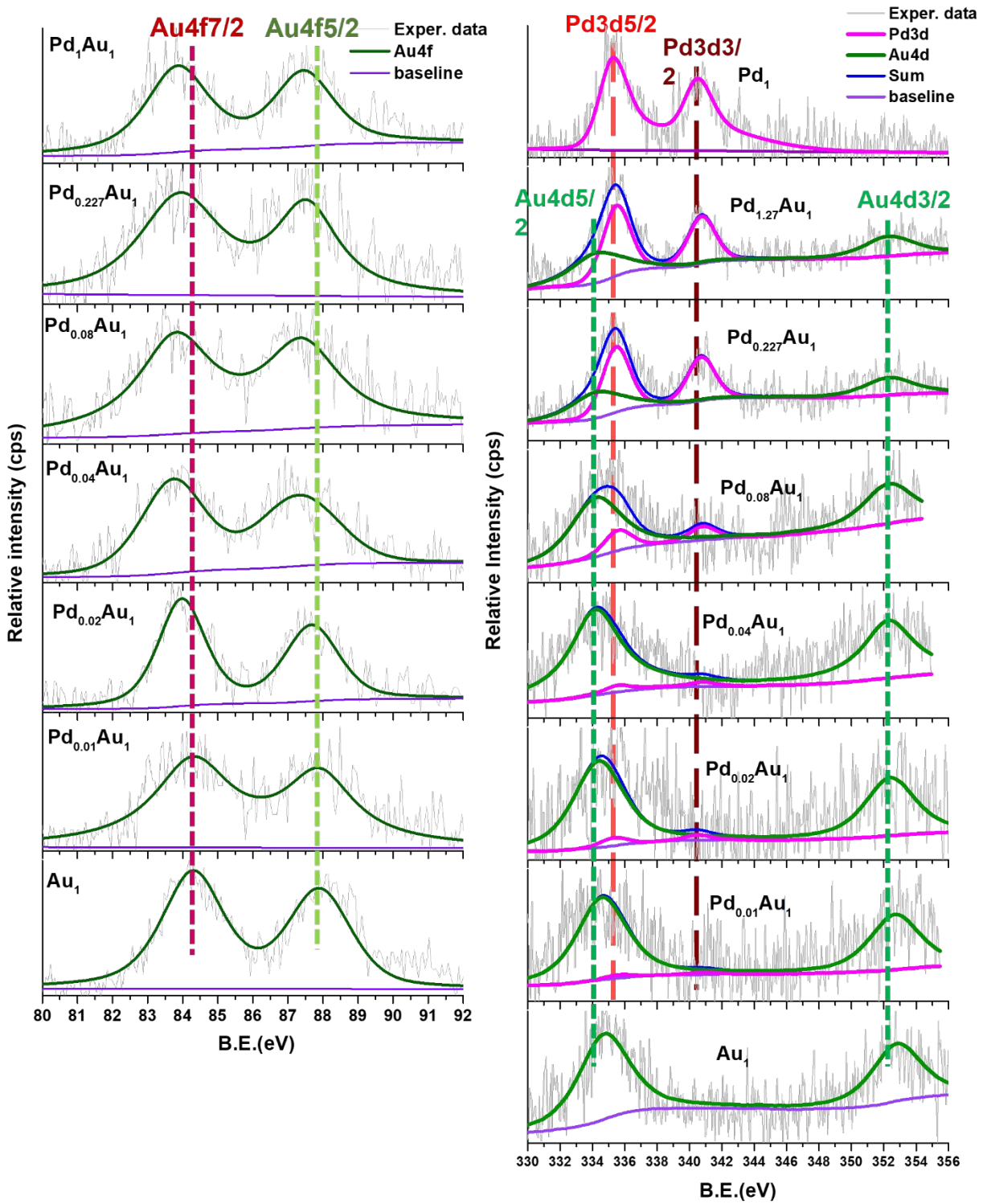

356

357 Figure 4. XPS spectra comparison of Au4f (a), Pd3d and Au3d (b) over PdAu DLA catalysts.

358

The characterization to this point indicates that the co-SEA yields well alloyed PdAu nanoparticles with, at the dilute limit, about thirty-five to forty percent of the Pd atoms at the surface. In addition, the Pd and Au are in close enough proximity to allow electron transfer. A final characterization is the use of CO-FTIR to determine to what extent the surface Pd is isolated or exists as ensembles.

The PdAu DLA system is an ideal system to characterize Pd site isolation by CO-FTIR; the matrix of Au will not adsorb CO in appreciable amounts, and Pd in ultrasmall nanoparticles adsorb CO mostly in bridged and hollow sites [40, 41]. Thus, the disappearance of bridged and hollow-adsorbed CO on Pd, which appears below 2000 cm^{-1} [42, 43], with the persistence of linear-adsorbed CO (bands above 2000 cm^{-1}), without any interference from CO adsorption on the second metal, is a sensitive probe of Pd site isolation [42]. The procedure for collecting spectra over an equilibrated surface is illustrated in Figure S4 for the $Pd_{1.27}Au_1$ catalyst. Flowing 1% CO in Ar for 30 minutes caused a gradual increase in the adsorbed CO bands (gas phase removed for clarity in Figure S4c) and afterwards, CO is removed from the gas stream and the adsorbed species re-equilibrate (Figures S4b and d). After purging CO from the gas phase, the linear CO peaks decreased a bit while the bridged and hollow-bound CO peaks remained relatively constant. These spectra were

acquired with an *in-situ* reduction of 180 °C (instead of 400 °C) which completely eliminated the uptake of CO onto Au. The final equilibrated spectrum of this and all the other samples comprise Figure 5.

The CO-FTIR spectra of the series of single metal and bimetallic catalysts, following the 180 °C in-situ reduction (which followed a prior 400 °C reduction and handling in air to press the IR discs) is shown in Figure 5. The pure Au is shown in the bottom spectrum, and pure Pd samples are shown in the top two spectra. No CO was observed on the monometallic Au catalyst following the lower temperature reduction. Besides the monometallic $Pd_{0.97}$ sample, another Pd-only sample ($Pd_{0.10}$) was made, specifically for the IR study, with a lower Pd loading more representative of the Pd loadings in the DLA catalysts. The SEA-derived 0.10 wt% Pd sample corresponds to the amount of Pd present in the $Pd_{0.08}Au_1$ sample. Both of these samples show a set of linear adsorption peaks above 2000 cm^{-1} and a set of multiply-bonded peaks below 2000 cm^{-1}. Gaussian fitting revealed for both samples the three characteristic linearly adsorbed CO bands (L1, L2, L3) in the regime of 2100-2000 cm^{-1}, centering around 2088 cm^{-1}, 2072 cm^{-1} and 2040 cm^{-1}, which can be ascribed to linear carbonyls on terrace, edges and kinks sites on Pd [111] and [200] facets [42, 44-46]. The bridged CO stretching region with lower frequency [47] can be curve fit with peaks at

around 1965 cm^{-1} (B1) and 1890 cm^{-1} (B2), ascribed CO bridge-bonded to pairs of Pd atoms on [111] and [200] facets [48, 49]. In addition, another two stretching bands at 1850 cm^{-1} (H1), and 1779 -1744 cm^{-1} (H2), are required to finely fit the spectra due to CO bonded on three-fold hollow Pd sites on [111] and more open facets[41, 49]. The latter sites only appear on the higher loading Pd-only catalyst, perhaps from a larger particle size. Assignments of IR peaks are summarized in Table 5.

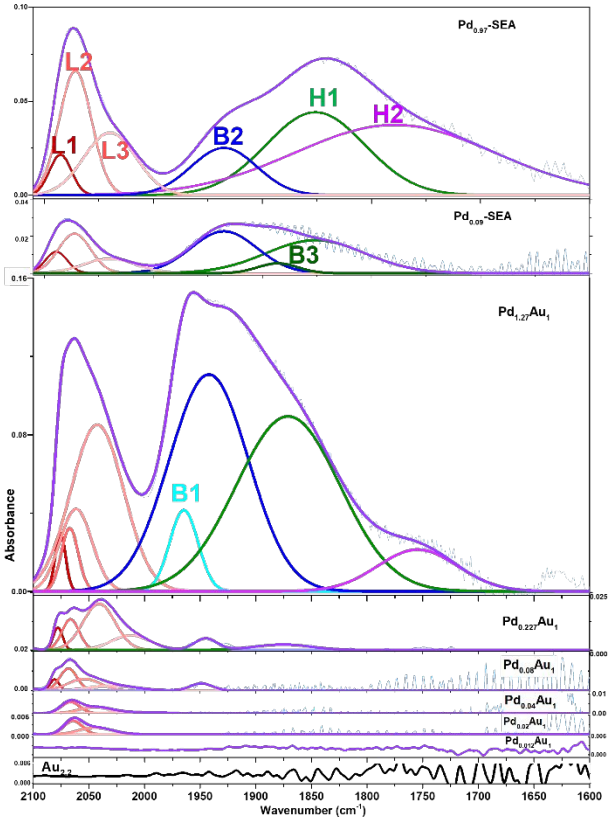

Figure 5. IR spectra over monometallic and PdAu DLA catalysts.

401

402

403

404

405

406

407

408

409

410

411 Table 5. Assignments of CO adsorption on Pd sites over monometallic and PdAu DLA catalysts.

Samples	Linear-CO on Pd (cm^{-1})			bridged CO on Pd (cm^{-1})			3-hollow CO (cm^{-1})		Linear CO fraction (%)
	L1, L1'	L2	L3	B1	B2	B3	H1	H2	
	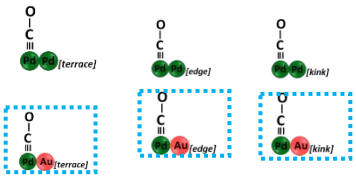								
$Pd_{0.97}$_SEA	2085	2071	2040	---	1935	---	1851	1779	24
$Pd_{0.10}$_SEA	2089	2072	2040	---	1935	1886	1851	---	28
$Pd_{1.27}Au_1$_co-SEA	2075 2063	2047	---	1966	1936	1896	---	1744	25
$Pd_{0.23}Au_1$_co-SEA	2078 2063	2040	2019	1946	---	---	---	---	81
$Pd_{0.08}Au_1$_co-SEA	2080 2063	2040	2022	1948	---	---	---	---	88

$Pd_{0.04}Au_1$_co-SEA	2063	2045	2013	---	---	---	---	---	100
$Pd_{0.02}Au_1$_co-SEA	2063	2042	2017	---	---	---	---	---	100
reference	2069 [11] 2065 [39, 47]	2078 [46]		1950 [11, 39, 47]	1940 [43]	1900 [43]	1859 [47] 1820 [43]	1755 [47]	

412 *: CO bands in the blue rectangles corresponds to the cartoon figures in the blue rectangles.

413

414 Both Pd-only catalysts show a majority of bridged or hollow-bound CO, and with about
415 the same fraction (24-28%) of linear species. Interestingly, the high Pd loading ($Pd_{1.27}Au_1$) sample
416 also shows a high percentage of nonlinear sites, with an abundance of bridged sites and a decrease
417 of hollow sites compared to the Pd-only catalysts. Curve fitting the linear carbonyl region in this
418 spectrum gives a new CO band at 2063 cm^{-1}, which can be ascribed to linearly bonded-CO on
419 isolated Pd sites associated with Au [11,42,50]. The red shift of 7-30 cm^{-1} in linear carbonyl frequency
420 might be interpreted by two factors: less competition in the anti-bonding π-back-donation from Au
421 than Pd [50]; or weakened dipole-dipole coupling because of the decreased amount of CO molecules
422 adsorbed on the diluted Pd sites [11,50,51]. The red shifts of the multi-adsorption IR peaks could be
423 also explained by the effects of the alloys and/or CO coupling.

424 Starting with the $Pd_{0.227}Au_1$ sample, the intensity of the bridge and hollow-bound peaks
425 diminishes rapidly until they disappear completely at the 0.04:1 ratio. An analysis based on the

area of IR-spectra resolved peaks can be used to quantify the fraction of isolated Pd on Au surface [20,40]; a comparison of the ratios of linear peak intensity to total intensity is shown in Figure 6. While the Pd-rich sample ($Pd_{1.27}Au_1$) shows about the same ratio of linear species as the Pd-only samples, the percentage of linear species raises rapidly in the lower loading samples and appears to be 100% at or below 0.04:1 Pd:Au. As about 60 % of the Pd in that sample is alloyed in the bulk and not on the surface (Table 2), the effective surface ratio of Pd is 0.016:1, or about 1 Pd:63 Au. Per the Hartog/van Hardeveld relation [32], a 1.7 nm nanoparticle contains about 120 atoms, and at 0.04:1 Pd, Au, it would contain about 5 atoms of Pd, of which about 2 would exist at the surface. Lower Pd/Au ratios would contain correspondingly lower numbers of total and surface Pd per nanoparticle.

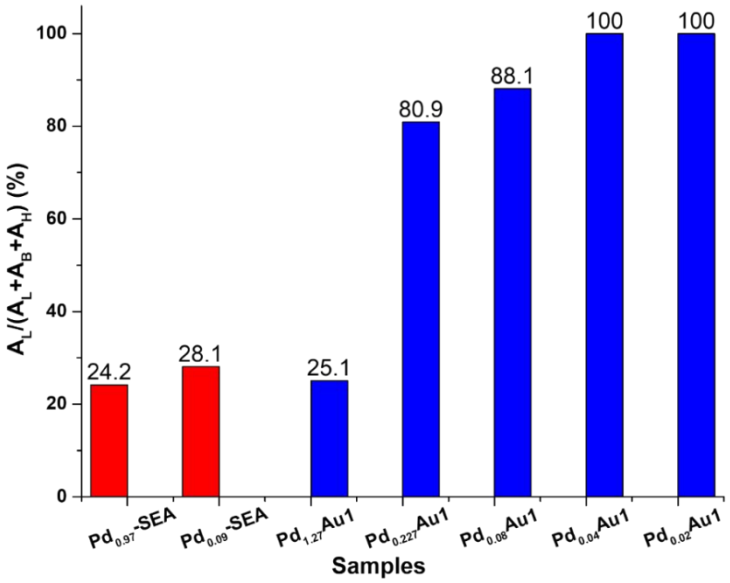

Figure 6. CO-FTIR estimated the fraction of linearly adsorbed CO bands.

The density of isolated surface sites of Pd in the gold matrix, obtained by this simple synthesis, is reasonably high. Filie and the co-workers[52] used a colloidal preparation of bimetallic nanoparticles and noted a dual-site mechanism over their dilute Pd-in-Au alloys on SiO_2 at 1:50 Pd:Au due to the presence of both clustered and isolated Pd sites, suggesting partial isolation of surface Pd atoms. Ricciardulli et al.[53] synthesized catalysts with a sequence of SEA of Au ethylenediamine followed by electroless deposition of Pd, and reported the initial isolation of Pd at an Au/Pd ratio of 37, although bridged CO did appear in this and a 50:1 sample after prolonged annealing in CO at 100 °C. Both of these works employed nanoparticles of larger size, about 6 and 7 nm, respectively, than the 1.7 nm particles produced here via co-SEA.

3.2 Partial Oxidation of 1-phenylethanol

The probe reaction chosen to test the effect of isolated Pd in the Au matrix was the partial oxidation (or dehydrogenation) of 1-phenylethanol to acetophenone. The oxidation of alcohols is an important class of catalytic processes to obtain value-added fine chemicals[54]. For this class of reactions the support has been shown to have a substantial effect on the reactivity, with activity on silica among the lowest reported[55,56]. Therefore, the effect of Pd isolation in Au should appear most prominently over this support. As high temperatures can catalyze the cleavage of C-C bond in the alcohol and lead to a low selectivity to the desired aldehyde[50,57] a low temperature at 160 °C was employed. At this temperature and with 50 psig oxygen, selectivity to acetophenone was 100%.

Figure 7a shows results from a series of catalysts for which the mass of catalyst was adjusted to give the same number of total Pd sites, 0.64 mmol of Pd (except for the Au-only catalyst, which contained 0.64 mmol of Au.) Both pure metals exhibited low activity. Placing the same amount of Pd into the Au lattice at the ratio of 0.227:1 gave a much more active catalyst, and diluting the same amount of Pd even further to 0.08:1 increased the activity further. While it is typical to attribute reactivity of alcohol oxidation over Pd/Au catalysts to both metals[38,39,55,58,59], the relative activity of the two metals in the alloyed particles might be surmised from this comparison. Both catalysts contained the same amount of Pd, while the $Pd_{0.08}Au_1$ sample contained 2.8 times more Au than $Pd_{0.227}Au_1$. The activity of the latter catalyst was only

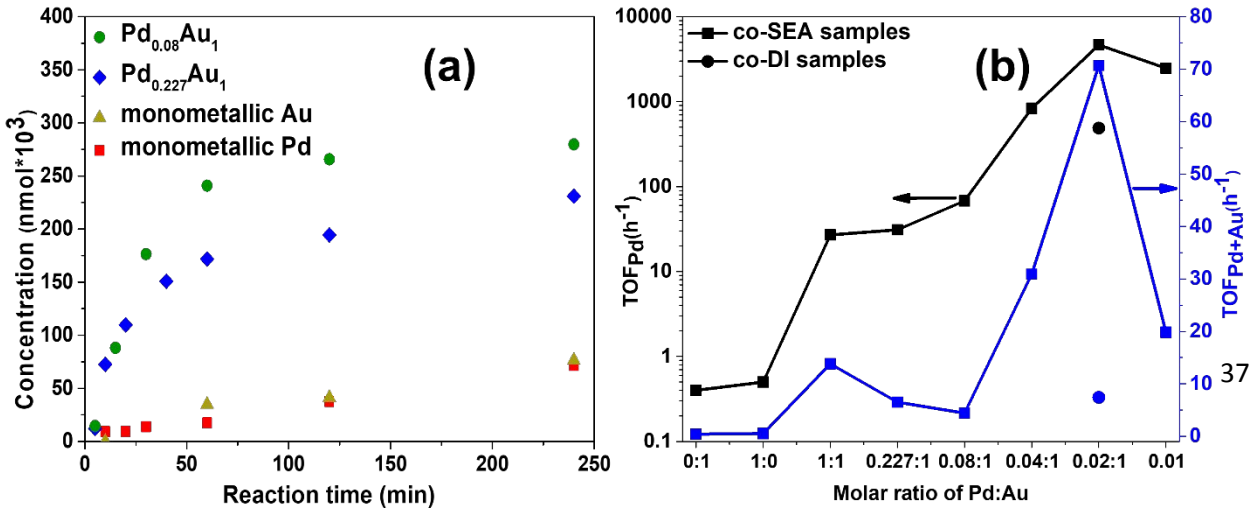

about 10% higher than that of the $Pd_{0.227}Au_1$ catalyst with three times less Au. This suggests that the main catalytic site in the reaction is Pd, and the role of Au is to modify it.

Figure 7. (a) Concentration of acetophenone per 0.64 mmol Pd vs reaction time (0.64 mmol Au for monometallic Au); (b) turnover frequency based on total Pd and total (Pd + Au).

Runs with the remaining DLA catalysts (at lower Pd:Au ratios) could not be conducted with a constant amount of Pd due to the low amounts of Pd in the remainder of the series, so a constant mass of 106 mg was used and the high Pd dilutions were rerun with this sample mass. Measured rates converted to turnover frequency based on Pd only and total metal are summarized in Table 6 and plotted in Figure 7b. The turnover frequency based solely on Pd increases four orders of magnitude as the Pd is isolated into the Au matrix, with the samples shown by IR to be totally isolated (0.04 and lower) to be the most active by 1 to 2 orders of magnitude over catalysts showing small ensembles of Pd (1:1 – 0.08:1) and these in turn are almost two orders of magnitude higher in activity than pure Pd or Au. As the Pd dispersions of the DLA catalysts are about the same (Table 2) and are lower than the pure Pd (1 nm particles have about 100% dispersion), an alternate calculation of turnover frequency based on surface Pd would show the same trend, or in the case of pure Pd, an even greater difference in activity.

Table 6. Summary of TOFs based on Pd only and total metal (Pd+Au)

molar ratio Pd/Au	Rate mmol/g_{cat}h	Pd (μmol/L)	Au (μmol/L)	TOF_{Pd} (1/h)	TOF_{Pd+Au} (1/h)
0:1	110	0	248	0.40	0.40
1:0	94	194	0	0.50	0.50
1:1	797	230	230	27	13.5
0.227:1	1850	32	204	31	5.2
0.08:1	1240	18	258	68	4.4
0.04:1	445	10.	258	833	30.9
0.02:1	1780	4.0	248	4650	74
0.01:1	469	2.0	248	2480	19.8
(co-DI) 0.02:1	258	5.5	248	488	10.6

Turnover frequencies based on total metal loading are seen in Figure 7b from the right-hand axis. These show activities higher by one to two orders of magnitude compared to the single metals, with the highest TOF for the $Pd_{0.02}Au_1$ sample. The $Pd_{0.02}Au_1$ sample prepared by co-dry impregnation as a control (presumably with larger particles and poorer alloying), had a much lower TOF. The maximum TOF at high Pd dilution seen in both curves has also been observed in several studies of Pd/Au alloys for glycerol oxidation[38,58,59]. In prior studies of series of Pd/Au alloys for 1-phenylethanol oxidation, activity maxima have been reported close to 1:1 Pd/Au[37,39], although neither of these studies tested dilute Pd alloys. In Figure 7b, there is also a slight downturn in TOF past 1:1, similar to those trends, but then there is another maximum at high dilution which far

494 exceeds the first maximum. This second maximum suggests a second kinetic regime, the study of
495 which is beyond the scope of this paper.

496 Li et al.[60] utilized DFT simulation and found that in the dehydrogenation of ethanol over
497 isolated Pd atoms in a Au [111] surface, the activation barrier for α-C-H cleavage is lower than O-
498 H bond scission and the dissociated H atom migrates to the 3-fold hollow sites with one isolated
499 Pd and two adjacent Au atomic ensemble, while *β*-C-H mainly adsorbed on Au sites with high
500 energy barrier. That interpretation is not inconsistent with the current results. That the 0.227:1 and
501 the 0.08:1 Pd:Au catalysts are up to two orders of magnitude less active than the lower Pd/Au
502 ratios, even though there is relatively little multiply-bound CO (Figures 5 and 6) in these catalysts,
503 suggests that the main increase in activity stems from an electronic effect of isolated Pd atoms;
504 surrounding the Pd with more Au helps. The charge transfer observed here from Pd to Au in the
505 alloys has been shown to facilitate the generation of gold anions which can easily adsorb O_2 [61]. It
506 is perhaps in the more dilute samples that this local environment is optimized.

507

508 **4. CONCLUSIONS**

509 Dilute Pd-in-Au homogenous alloys with ultra-small nanoparticles can be readily
510 synthesized via simultaneous electrostatic adsorption. The ratio of metals is easily controlled using

the concentration of the metal precursors in the impregnating solution. The nanoparticles generated from this synthesis appear to be largely alloyed, with the fraction of Pd on the surface about equal to the total metal dispersion. Pd atoms appear to become completely isolated at or below a Pd:Au ratio of 0.04:1 or 1:25, with 35 to 40% of these being present at the surface and available for reaction. The turnover frequencies for 1-phenylathanol dehydrogenation to acetophenone of the DLA series increased up to two orders of magnitude or more as the Pd atoms were successively diluted in a Au matrix.

ASSOCIATED CONTENT

Supporting Information

The supporting information is uploaded as a separate file, including TPR, XRD data, STEM images, and FTIR plots.

CORRESPONDING AUTHOR

John R. Regalbuto – University of South Carolina, Columbia, South Carolina 29208, United States.

*Email: regalbuj@cec.sc.edu

ACKNOWLEDGEMENTS

The authors acknowledge the financial support from National Science Foundation (IIP-1939876).

REFERENCES

1. Gates, B. C.; Flytzani-Stephanopoulos, M.; Dixon, D. A.; Katz, A., Atomically dispersed supported metal catalysts: perspectives and suggestions for future research. *Catalysis Science & Technology* **2017,** 7 (19), 4259-4275.

2. Kim, D.; Resasco, J.; Yu, Y.; Asiri, A. M.; Yang, P., Synergistic geometric and electronic effects for electrochemical reduction of carbon dioxide using gold-copper bimetallic nanoparticles. *Nature communications* **2014,** *5*, 4948-5955.

3. Kuo, C.-T.; Lu, Y.; Kovarik, L.; Engelhard, M.; Karim, A. M., Structure Sensitivity of Acetylene Semi-Hydrogenation on Pt Single Atoms and Subnanometer Clusters. *ACS Catalysis* **2019,** 9 (12), 11030-11041.

4. Liu, J.; Lucci, F. R.; Yang, M.; Lee, S.; Marcinkowski, M. D.; Therrien, A. J.; Williams, C. T.; Sykes, E. C.; Flytzani-Stephanopoulos, M., Tackling CO Poisoning with Single-Atom Alloy Catalysts. *Journal of the American Chemical Society* **2016,** 138 (20), 6396-6399.

5. Simonovis, J. P.; Hunt, A.; Palomino, R. M.; Senanayake, S. D.; Waluyo, I., Enhanced Stability of Pt-Cu Single-Atom Alloy Catalysts: In Situ Characterization of the Pt/Cu(111) Surface in an Ambient Pressure of CO. *The Journal of Physical Chemistry C* **2018,** 122 (8), 4488-4495.

6. Zhang, X.; Cui, G.; Feng, H.; Chen, L.; Wang, H.; Wang, B.; Zhang, X.; Zheng, L.; Hong, S.; Wei, M., Platinum-copper single atom alloy catalysts with high performance towards glycerol hydrogenolysis. *Nature communications* **2019,** 10 (1), 5812-5823.

7. Chen, Z.; Zhang, P., Electronic Structure of Single-Atom Alloys and Its Impact on The Catalytic Activities. *ACS Omega* **2022,** *7* (2), 1585-1594.

8. Pei, G. X.; Liu, X. Y.; Wang, A.; Lee, A. F.; Isaacs, M. A.; Li, L.; Pan, X.; Yang, X.; Wang, X.; Tai, Z.; Wilson, K.; Zhang, T., Ag Alloyed Pd Single-Atom Catalysts for Efficient Selective Hydrogenation of Acetylene to Ethylene in Excess Ethylene. *ACS Catalysis* **2015,** *5* (6), 3717-3725.

9. Mamatkulov, M.; Yudanov, I. V.; Bukhtiyarov, A. V.; Neyman, K. M., Pd Single-Atom Sites on the Surface of PdAu Nanoparticles: A DFT-Based Topological Search for Suitable Compositions. *Nanomaterials,* **2021,** *11* (1), 1-17.

10. Hannagan, R. T.; Giannakakis, G.; Flytzani-Stephanopoulos, M.; Sykes, E. C. H., Single-Atom Alloy Catalysis. *Chemical reviews* **2020,** 120 (21), 12044-12088.

11. Pei, G. X.; Liu, X. Y.; Wang, A.; Li, L.; Huang, Y.; Zhang, T.; Lee, J. W.; Jang, B. W. L.; Mou, C.-Y., Promotional effect of Pd single atoms on Au nanoparticles supported on silica for the selective hydrogenation of acetylene in excess ethylene. *New Journal of Chemistry* **2014,** *38* (5), 2043-2051.

12. Liu, J.; Uhlman, M. B.; Montemore, M. M.; Trimpalis, A.; Giannakakis, G.; Shan, J.; Cao, S.; Hannagan, R. T.; Sykes, E. C. H.; Flytzani-Stephanopoulos, M., Integrated Catalysis-Surface Science-Theory Approach to Understand Selectivity in the Hydrogenation of 1-Hexyne to 1-Hexene on PdAu Single-Atom Alloy Catalysts. *ACS Catalysis* **2019,** *9* (9), 8757-8765.

570 13. Reocreux, R.; Uhlman, M.; Thuening, T.; Kress, P.; Hannagan, R.; Stamatakis, M.; Sykes,
571 E. C. H., Efficient and selective carbon-carbon coupling on coke-resistant PdAu single-atom
572 alloys. *Chemical communications* **2019,** *55* (100), 15085-15088.

573 14. Liu, J.; Shan, J.; Lucci, F. R.; Cao, S.; Sykes, E. C. H.; Flytzani-Stephanopoulos, M.,
574 Palladium–gold single atom alloy catalysts for liquid phase selective hydrogenation of 1-hexyne.
575 *Catalysis Science & Technology* **2017,** *7* (19), 4276-4284.

576 15. Lee, J. D.; Miller, J. B.; Shneidman, A. V.; Sun, L.; Weaver, J. F.; Aizenberg, J.; Biener,
577 J.; Boscoboinik, J. A.; Foucher, A. C.; Frenkel, A. I.; van der Hoeven, J. E. S.; Kozinsky, B.;
578 Marcella, N.; Montemore, M. M.; Ngan, H. T.; O'Connor, C. R.; Owen, C. J.; Stacchiola, D. J.;
579 Stach, E. A.; Madix, R. J.; Sautet, P.; Friend, C. M., Dilute Alloys Based on Au, Ag, or Cu for
580 Efficient Catalysis: From Synthesis to Active Sites. *Chemical reviews* **2022,** 122 (9), 8758-8808.

581 16. Wrasman, C. J.; Riscoe, A. R.; Lee, H.; Cargnello, M., Dilute Pd/Au Alloys Replace Au/TiO2
582 Interface for Selective Oxidation Reactions. *ACS Catalysis* **2020,** 10 (3), 1716-1720.

583 17. Zhang, T.; Walsh, A. G.; Yu, J.; Zhang, P., Single-atom alloy catalysts: structural analysis,
584 electronic properties and catalytic activities. *Chemical Society reviews* **2021,** 50 (1), 569-588.

18. A. Wong, Q. L., S. Griffin, A. Nicholls, J. R. Regalbuto*, Synthesis of ultrasmall, homogeneously alloyed, bimetallic nanoparticles on silica supports. *Science* 2017, 358 , 1427–1430 (2017).

19. Regalbuto, J. R., Catalyst Preparation: Science and Engineering. *CRC Press* 2006.

20. De Castro, L.; Sahsah, D.; Heyden, A.; Regalbuto, J.; Williams, C., Dilute Limit Alloy Pd–Cu Bimetallic Catalysts Prepared by Simultaneous Strong Electrostatic Adsorption: A Combined Infrared Spectroscopic and Density Functional Theory Investigation. *The Journal of Physical Chemistry C* 2022, 126 (27), 11111-11128.

21. Block B.P., Bailar J.C. JR., The Reaction of Gold(III) with Some Bidentate Coordinating Groups. *Gold(III) with Some Bidentate Coordinating Group* 1951, 73, 4722-4725.

22. Sean R. Noble, S. E. B., Ritubarna Banerjee a, Jeff Miller, John R. Regalbuto Supported nanoparticle synthesis with Au bis-Ethylenediamine: The mechanism of adsorption onto oxides and carbons. *Journal of Catalysis* 2021, 393, 344–356.

23. O'Connell, K.; Regalbuto, J. R., High Sensitivity Silicon Slit Detectors for 1 nm Powder XRD Size Detection Limit. *Catalysis Letters* 2015, 145 (3), 777-783.

600 24. Banerjee, R.; Regalbuto, J. R., Rectifying the chemisorption – XRD discrepancy of carbon
601 supported Pd: Residual chloride and/or carbon decoration. *Applied Catalysis A: General* **2020,** 595
602 (117504), 1-10.

603 25. Rakočević, L.; Srejić, I.; Maksić, A.; Golubović, J.; Štrbac, S., Hydrogen Evolution on
604 Reduced Graphene Oxide-Supported PdAu Nanoparticles. *Catalysts* **2021,** 11 (481), 1-12.

605 26. Riahi G., Guillemot D. Polisset-Thfoin M., Khodadadi A.A, Fraissard J., Preparation,
606 characterization and catalytic activity of gold-based nanoparticles on HY zeolites. *Catalysis Today*
607 2002, 72, 115–121.

608 27. Lipp. J, Banerjee, R., Patwary M.D.F., Patra N., Dong A., Girgsdies, F., Bare S., Regalbuto J.,
609 The Extension of Rietveld Refinement for Benchtop Powder XRD Analysis of Ultra-small
610 Supported Nanoparticles. *Chemistry of Materials* 2022, in press.

611 28. Miller, J. T.; Kropf, A. J.; Zha, Y.; Regalbuto, J. R.; Delannoy, L.; Louis, C.; Bus, E.; van
612 Bokhoven, J. A., The effect of gold particle size on AuAu bond length and reactivity toward
613 oxygen in supported catalysts. *Journal of Catalysis* **2006,** 240 (2), 222-234.

614 29. Denton, A. R.; Ashcroft, N. W., Vegard's law. *Physical Review A* **1991,** *43* (6), 3161-3164.

30. Leppert, L.; Albuquerque, R. Q.; Kümmel, S., Gold-platinum alloys and Vegard's law on the nanoscale. *Physical Review B* **2012,** *86* (241403), 241403-1 – 241403-5.

31. Qian, K.; Luo, L.; Jiang, Z.; Huang, W., Alloying Au surface with Pd reduces the intrinsic activity in catalyzing CO oxidation. *Catalysis Today* **2017**, 280, 253-258.

32. Hartog, R., Van Hardeveld, A. F., The Statistics of Surface Atoms and Surface Sites on Metal Crystals. *Surface Science* **1969,** 15, 189-230.

33. C.-W. Yi, K. L., T. Wei, and D. W. Goodman, The Composition and Structure of Pd-Au Surfaces. *The Journal of Physical Chemistry B* ***2005,*** 109, 18535-18540.

34. Tiruvalam, R. C.; Pritchard, J. C.; Dimitratos, N.; Lopez-Sanchez, J. A.; Edwards, J. K.; Carley, A. F.; Hutchings, G. J.; Kiely, C. J., Aberration corrected analytical electron microscopy studies of sol-immobilized Au + Pd, Au{Pd} and Pd{Au} catalysts used for benzyl alcohol oxidation and hydrogen peroxide production. *Faraday Discuss* **2011,** 152, 63-86.

35. Gallo, I. B. C.; Carbonio, E. A.; Villullas, H. M., What Determines Electrochemical Surface Processes on Carbon-Supported PdAu Nanoparticles? *ACS Catalysis* **2018,** 8 (3), 1818-1827.

36. Kaden, W. E., Electronic structure controls reactivity of size-selected Pd clusters adsorbed on TiO2 surfaces. *Science* **2009**, 326 (5954), 826-829.

37. Nishimura, S.; Yakita, Y.; Katayama, M.; Higashimine, K.; and Ebitani, K.; The role of negatively charged Au states in the aerobic oxidation of alcohols over hydrotalcite supported AuPd nanoclusters, *Catalysis Science and Technology* **2013**, 3, 351-359.

38. Li, J.; Xu, Y.; Wang, S.; and Zhang, H., Ultrafine AuPd nanoclusters on layered double hydroxides by the capt-capped AuPd cluster precursor method: synergistic effect for highly efficient aerobic oxidation of alcohols, *The Journal of Physical Chemistry C* **2019**, 123, 15483-94.

39. Chang, J.B.; Liu, C.H.; Liu, J.; Zhou, Y.-Y.; Gao, X.; and Wang, S.D., Green-chemistry compatible approach to TiO2-supported PdAu bimetallic nanoparticles for solvent-free 1-Phenylethanol oxidation under mild conditions, *Nano-Micro Letters*, **2015**, 7(3) 307-315.

40.Griselda, C.; Cabilla, A.; Albama, A., Characterization by CO/FTIR spectroscopy of Pd/silica catalysts and its correlation with syn-gas conversion. *Catalysis Letters **1998**,* 55, 147–156.

41. Tereshchenko, A.; Guda, A.; Polyakov, V.; Rusalev, Y.; Butova, V.; Soldatov, A., Pd nanoparticle growth monitored by DRIFT spectroscopy of adsorbed CO. *Analyst* **2020,** 145 (23), 7534-7540.

42. Luneau, M.; Shirman, T.; Filie, A.; Timoshenko, J.; Chen, W.; Trimpalis, A.; Flytzani-Stephanopoulos, M.; Kaxiras, E.; Frenkel, A. I.; Aizenberg, J.; Friend, C. M.; Madix, R. J., Dilute Pd/Au Alloy Nanoparticles Embedded in Colloid-Templated Porous SiO2: Stable Au-Based Oxidation Catalysts. *Chemistry of Materials* **2019,** 31 (15), 5759-5768.

43. Shan, J.; Giannakakis, G.; Liu, J.; Cao, S.; Ouyang, M.; Li, M.; Lee, S.; Flytzani-Stephanopoulos, M., PdCu Single Atom Alloys for the Selective Oxidation of Methanol to Methyl Formate at Low Temperatures. *Topics in Catalysis* **2020,** 63 (7-8), 618-627.

44. Rebelli, J.; Detwiler, M.; Ma, S.; Williams, C. T.; Monnier, J. R., Synthesis and characterization of Au–Pd/SiO_2 bimetallic catalysts prepared by electroless deposition. *Journal of Catalysis* **2010,** *270* (2), 224-233.

45. Duplan J., Praliaud H., Infrared determination of the accessible metallic surface of supported palladium containing ceria. *Applied Catalysis A: General* **1991**, (67), 325-335.

46. Palazov A., Kakinow G. Bonew Ch., Shopov D., Estimation of the number of CO molecules adsorbed in various modes on different crystal planes of alumina supported polycrystalline palladium. *Surface Science* **1987,** (188) 505-518.

47. Blyholder B., Molecular Orbital View of Chemisorbed Carbon Monoxide. *The Journal of Physical Chemistry* **1964**, 68 (10), 2772-2777.

48. Junling Lu, B. F., Coking- and Sintering-Resistant Palladium Catalysts Achieved Through Atomic Layer Deposition. *Science* **2012**, 335 (6073), 1205-1208.

49. Giorgi, J. B., FTIR-Study of CO adsorption on crystalline-silica-supported palladium partilces. *Surface Science* **2002**, 498 (1-2), L71-L77.

50. Ouyang, M.; Papanikolaou, K. G.; Boubnov, A.; Hoffman, A. S.; Giannakakis, G.; Bare, S. R.; Stamatakis, M.; Flytzani-Stephanopoulos, M.; Sykes, E. C. H., Directing reaction pathways via in situ control of active site geometries in PdAu single-atom alloy catalysts. *Nature communications* **2021,** *12* (1), 1549-1559.

670 51. Bradshaw, A., Hoffman F.M., The chemisorption of carbon monoxide on palladium single
671 crystal surfaces: IR spectroscopic evidence for localised site adsorption. *Surface Science 1978, 72*
672 *(3), 513-535.*

673 52. Filie, A.; Shirman, T.; Aizenberg, M.; Aizenberg, J.; Friend, C. M.; Madix, R. J., The
674 dynamic behavior of dilute metallic alloy Pd_xAu_{1-x}/SiO_2 raspberry colloid templated catalysts
675 under CO oxidation. *Catalysis Science & Technology* **2021,** *11* (12), 4072-4082.

676 53. Ricciardulli, T.; Gorthy, S.; Adams, J. S.; Thompson, C.; Karim, A. M.; Neurock, M.;
677 Flaherty, D. W., Effect of Pd Coordination and Isolation on the Catalytic Reduction of O2 to H2O2
678 over PdAu Bimetallic Nanoparticles. *Journal of the American Chemical Society* **2021,** *143* (14),
679 5445-5464.

680 54. Davis, S. E.; Ide, M. S.; Davis, R. J., Selective oxidation of alcohols and aldehydes over
681 supported metal nanoparticles. *Green Chemistry* **2013,** *15* (1), 17-45.

682 55. Enache, D.L.; Edwards, J.K.; Landon, P.; Solsana-Espriu, B.; Carley, A.F.; Herzing, A.A.;
683 Watanabe, M.; Kiely, C.J.' Knight, D.W.; and Hutchings, G.J., Solvent-free oxidtion of primary
684 alcohols to aldehydes using Au-Pd/TiO_2 catalysts, *Science* **2006**, 311, 362-365.

685 56. Villa, A.; Dimitratos, N.; Chan-Thaw, C.E.; Hammond, C.; Prati, L.; and Hutchings, G.J.,
686 Glyceraol Oxidation using gold-containing catalysts, *Accounts of Chemical Research* **2014**, 48
687 (5), 1403-1412.

688 57. Giannakakis, G.; Trimpalis, A.; Shan, J.; Qi, Z.; Cao, S.; Liu, J.; Ye, J.; Biener, J.; Flytzani-
689 Stephanopoulos, M., NiAu Single Atom Alloys for the Non-oxidative Dehydrogenation of Ethanol
690 to Acetaldehyde and Hydrogen. *Topics in Catalysis* **2018,** *61* (5-6), 475-486.

691 58. Wang, D.; Villa, A.; Porta, F.; Prati, L.; and Su, D., Bimetallic gold/palladium catalysts:
692 correlation between nanostructure and synergistic effects, T*he Journal of Physical Chemistry C*
693 **2008**, 112, 8617-8622.

694 59. Villa, A.; Campione, C.; and Prati, L., Bimetallic gold/palladium catalysts for the selective
695 liquid phase oxidtion of glycerol, *Catalysis Letters* **2007**, 115, 133-136.

696 60. Li, H.; Chai, W.; Henkelman, G., Selectivity for ethanol partial oxidation: the unique
697 chemistry of single-atom alloy catalysts on Au, Ag, and Cu(111). *Journal of Materials Chemistry*
698 *A* **2019,** *7* (41), 23868-23877.

61. Mitsutaka Okumura, Y. K., Masatake Haruta, Kizashi Yamaguchi, DFT studies of interaction between O_2 and Au clusters. The role of anionic surface Au atoms on Au clusters for catalyzed oxygenation. *Chemical Physics Letters* 2001, *346 (2001) 163-168*.